# Damage mechanisms in the CAI failure of thin z-pinned composite laminates

L. Francesconi[a] and F. Aymerich[b]

[a] Department of Mechanical Engineering, Santa Clara University, Santa Clara, CA, USA
now with Logitech Europe - EPFL, Lausanne (CH)
[b] Department of Mechanical, Chemical and Materials Engineering, University of Cagliari, Italy

**Abstract**

The results of an experimental investigation into the compression after impact (CAI) performance of thin z-pinned carbon-epoxy laminates are reported in this paper. Unpinned and z-pinned $[0_2/90_2]_S$ and $[0/\pm 45/90]_S$ samples were impacted at energies varying between 2 J and 35 J and then subjected to compression loading until failure. The amount and nature of the damage induced by impact and the damage mechanisms leading to CAI failure were characterized by X-radiography and through visual observation of the sample surfaces. The study shows that the effect of z-pins may be beneficial or detrimental to the post-impact strength of the laminates depending on the energy of the impact. The sequence of the main damage mechanisms observed on the laminates during the compression tests is illustrated and discussed to clarify the role of z-pins in controlling the residual strength of the impacted laminates over the full range of examined impact energies.

**Keywords:** A. 3-Dimensional reinforcement; B. Impact Behaviour; B. Damage Tolerance, z-pinning

## 1. Introduction

Fibre-reinforced laminated composites offer a number of advantages over more conventional materials, but are highly susceptible to delamination failures under impact events that may occur in service or during the manufacturing, installation and maintenance phases. Impact-induced delaminations may cause severe degradation of the structural properties and may result, especially under compressive loads, in the sudden collapse of the damaged component.

Among the various strategies proposed to improve the resistance to delamination of laminated composites [1, 2], one of the most effective approaches consists in inserting translaminar reinforcements in the form of continuous threads or yarns (stitching, tufting, 3D weaving) [3-5] or discontinuous fibres or pins (z-pinning) [6-11]. The beneficial effect is generated by the traction forces transmitted across the delamination crack by the through-thickness z-reinforcement, which resist crack opening and sliding, thereby increasing the resistance to crack growth [1, 10, 12]. As a direct result of the higher interlaminar fracture toughness, translaminar reinforcements offer substantial improvements to many mechanical properties of composite laminates, including impact resistance, damage tolerance, fatigue life, joint strength, etc. [1].

A significant amount of research work has been especially carried out on the effect of z-pinning on the delamination resistance of laminates [13]. Increases of more than one order of magnitude and up to five or six times were for example respectively reported for mode I and mode II interlaminar fracture resistance [9, 14] with relatively small volume content of z-pins (less than 4%). Similarly, large enhancements in the failure strength and energy absorption of lap, T-shaped and L-shaped composite joints were achieved by z-pinning across the bond surfaces [15-17]. The results of a number of investigations also show that z-pinning can significantly reduce the extent of the damage caused by low-velocity impact loads [6, 18-23], even though the benefits provided by z-pins were seen to depend on the level of impact energy and on the layup of the laminate. It was found, for example, that the improvements in delamination resistance increase with impact energy, due the fact that a large-scale bridging zone must develop ahead of the delamination front before significant toughening of the material can be achieved. Furthermore, z-pins become more effective in restraining impact delaminations with increasing laminate thickness [19], as a consequence of a change from bending failure in thin laminates (with damage initiated by matrix cracking at the back surface) to interlaminar shear failure (with internal damage dominated by delaminations at the interfaces close to the midplane) [24].

In contrast to the effort dedicated over the past decades to the characterization of the effect of z-pinning on the delamination resistance under low-velocity impacts, less work has been done to investigate the role of z-pins in the compression after impact (CAI) response of laminates.

Some preliminary work was carried out in the 1990s by Freitas and co-workers [25], who reported up to 50% improvements in the compressive residual strength of impacted carbon/epoxy panels after z-pinning. More recently, CAI tests were performed in [6, 18] on 4 mm thick quasi-isotropic carbon/epoxy laminates reinforced with carbon pins at densities of 0.5%, 2% and 4%. The samples were locally pinned either in a central square region or in a frame around the impact site. The CAI tests on laminates with a square pinned region showed improvements in the residual compressive strength of about 55% for laminates with 0.5% and 2% pin density and of up to 110% for laminates with 4% pin density in comparison with unpinned laminates. The CAI strength properties of samples with a frame-type pinning pattern were reported as better than those of control samples, even though not as good as those of samples with a central pinned area. Comparable trends were reported in [26] on quasi-isotropic laminates with similar square and frame pinning configurations.

The CAI behaviour of quasi-isotropic carbon/epoxy laminates with thicknesses of 4 mm and 6 mm, selectively reinforced with carbon pins in a central region at an areal density of 2%, was examined in [19]. Z-pinning was found to improve the CAI strength of the samples, with a residual strength approximately 45% higher than that of the unpinned counterparts. The failure of both unpinned and pinned samples occurred by the propagation of the impact-induced delamination caused by local buckling and the superior performances of z-pinned specimens over unpinned specimens were attributed to the smaller impact-induced damage size and to the delayed delamination growth during compression loading.

Quasi-isotropic and cross-ply composite laminates were investigated in [20, 27] to assess the influence of z-pinning on the post-impact compression behaviour of the laminates after low and high energy impacts. The experimental results show that while z-pins lead to CAI strength improvements of up to 20% on laminates subjected to high-energy impacts, they are not beneficial for laminates impacted at low energy levels, as a direct consequence of the inefficacy of z-pinning in enhancing delamination resistance in the presence of small damage.

In spite of the significant experimental evidence available for thick laminates (4 mm or thicker laminates were examined in the studies mentioned before), very few data are reported in the literature on the CAI response of thin z-pinned laminates. An exploratory analysis was carried out in [28] to compare the effect of z-pins on the CAI strength of laminates of different thicknesses (2, 4 and 7 mm). The study shows that pinning in thin laminates is much less beneficial to CAI strength than in thick laminates, thus indicating that the efficacy of z-pins is strongly related to the specific failure modes induced by impact.

Improvements in CAI strength up to 25% were achieved by Scharr and coworkers [22, 29] after reinforcing 3.5 mm thick quasi-isotropic carbon/epoxy laminates with plain or circumferentially notched z-pins. The samples were impacted with energies higher than 17 J and the main failure mode observed during CAI testing was delamination growth, which was however hindered by the bridging force of z-pins, thus accounting for the higher residual strength of pinned laminates.

The literature survey shows however that the current understanding on the CAI performance of z-pinned laminates is primarily based on experimental tests carried out over limited sets of impact energy levels, while there is a lack of data and observations covering the full range of the impact damage severities that may be induced by low velocity impacts. As a matter of fact, the role of z-pins on the mechanisms of compressive failure of impacted laminates is expected to be dependent on the characteristics and extent of the impact damage, which may vary from delamination initiation to perforation conditions involving

extensive fibre fracture. In addition, the rather different failure modes generated by impact loadings in thin and thick laminates suggest a specific characterization of the post impact performance of thin z-pinned laminates, which have up to now received very little attention in comparison to the more studied thick laminates.

With the aim of addressing these gaps, the study investigates the effect of z-pins on the compressive response of thin (2.5 mm) carbon/epoxy laminates impacted with energies between 2 and 35 J, chosen so as to introduce damage severities ranging from invisible or barely visible impact damage (BVID) up to complete through-thickness penetration. The sequences of failure and deformation events leading to CAI collapse, reconstructed by X-radiography and by direct observation of the surfaces of the samples during the CAI tests, are examined and compared to identify the mechanisms by which the z-pins control the compressive response of the laminates for the different damage conditions.

## 2. Experimental

Carbon/epoxy laminates with two stacking sequences, a cross-ply $[0_2/90_2]_S$ and a quasi-isotropic $[0/\pm45/90]_S$ layup, were examined in the study. The laminates were manufactured with Texipreg® HS300/ET223 unidirectional prepreg plies (62% fibre weight content) and consolidated under vacuum in autoclave at a pressure of 6 bar and a maximum temperature of 125 °C. Prior to curing, some of the panels were reinforced with carbon/BMI Z-FIBER© pins by ultrasonically assisted insertion. The pins had a diameter of 0.51 mm and were arranged in a square pattern with a spacing of 3.1 mm between adjacent pins, corresponding to an areal density of 2%. The panels were pinned on rectangular regions 20 mm by 60 mm in size and, after curing, samples 65 mm × 88 mm in size were cut from the panels to obtain samples with a z-pinned area centred on the impact point (fig. 1). The longer side of the rectangular pinned region was oriented along the 0° direction, which corresponds to the main growth direction of the impact-induced damaged area of the examined layups. The average thickness of the laminates was 2.5 mm, with no significant differences between z-pinned and unpinned laminates.

The impact tests were performed using an instrumented drop weight testing machine equipped with a 2.28 kg impactor. The samples were impacted with energies ranging between 2 J and 35 J, which correspond to impact velocities varying between 1.3 and 5.5 m/s. The range of impact energies was chosen in order to achieve damage severities extending from the onset of delamination up to full penetration of the indentor through the laminate thickness. During the impact tests, the specimens were supported on a steel frame

with a 45 mm × 68 mm rectangular opening and the desired energy was obtained by selecting the appropriate drop height of the impactor. Four soft rubber clamps were used to restrain the specimen to the support frame so as to inhibit rigid body motion during the impact.

The impact-damaged specimens were then loaded in compression using an anti-buckling fixture that provides support to the lateral edges of the specimen to prevent global buckling during application of the load. All CAI tests were performed under displacement control at a 1 mm/min rate in a 250 kN Instron servoelectric testing machine.

With reference to the size chosen for the samples, it should be observed that available standards and guidelines for CAI tests typically refer to laminates with thicknesses larger than 4 mm, for which a sample size of 100 mm × 150 mm is often suggested (see for example ASTM Standard D7137-12 [30]). Because of the small thickness of the laminates under investigation, a scaled down size of 65 mm x 88 mm was chosen in order to prevent global instability during the compression tests without the need of frontal anti-buckling supports that may interfere with the growth of damage, such as plates with a cut-out opening [31] or with vertical ribs [32].

Small fibreglass tabs were bonded to the loaded ends of the impacted specimens before CAI testing to avoid potential crushing damage. Despite this precaution, crushing failure always occurred at one of the loading edges in samples not subjected to impact. For this reason, only results on impacted samples, where the CAI failure initiates at the damaged region, are illustrated and discussed in the following section.

The extent and the features of the internal damage after both impact and CAI tests were characterized by penetrant enhanced X-radiography. The radiographic images were obtained on Agfa NDT D4 films using a Faxitron 43855A cabinet with the following settings: 20 kVp voltage, 3 mA tube current, and 100 s exposure time for an X-ray source to film distance of 60 cm.

A summary of the samples tested in the study is provided in Table 1.

## 3. Results and discussion

The damage response to low-velocity impacts of unpinned and pinned $[0_2/90_2]_S$ and $[0/\pm 45/90]_S$ laminates was investigated in a previous study and only a brief summary of the main findings relevant to the present analysis is provided here. A detailed description of the impact behaviour of the laminates may be found in [23].

Two main damage scenarios were observed in the impacted laminates depending on the level of impact energy. The damage generated by impacts in the low to intermediate regime (i.e. below approximately 15 J) predominantly consists of matrix cracking and delaminations, mostly occurring at the interfaces located near the rear side of the sample. By contrast, impacts with higher energy cause perforation damage, where extensive fibre fracture develops at the indentation region of the sample, in addition to large delaminations at various interfaces. Fibre failures initiate at impact energies of about 15 J (12 J for unpinned $[0_2/90_2]_S$ laminates) and, with increasing energy levels, progress from the impact side to the rear side of the laminate leading to complete penetration of the indentor into the sample. X-radiographs of typical damage patterns induced by low (2 J), intermediate (8 J) and high (30 J) energy impacts are shown in fig. 2. The areas of the projected delaminations induced by impact are plotted as a function of impact energy in the graphs of fig. 3, which also display the ranges of impact energy that produce perforation damage conditions. The data reported in the graphs show that the improvements in delamination resistance achieved by z-pinning depend on the energy of the impact. It was observed, in particular, that z-pins are not capable of delaying the initiation of delamination and become effective in reducing the size of interlaminar damage only when the delaminations are sufficiently large to allow the development of a large-scale crack bridging zone. The dependence of the efficacy of through-thickness reinforcements on the size of delaminations is a well-known effect that has been reported in various experimental studies on translaminar reinforced laminates [4, 11, 19-23]. It may be also worth mentioning that noticeable improvements in mode II fracture toughness with increasing strain rates have been reported in z-pinned carbon laminates [33]. The impact velocity could thus play some role in the effect of z-pins on the resistance to delamination growth exhibited by the laminates.

Representative stress vs displacement curves recorded during CAI tests on samples impacted at different energies are shown in the graphs of fig. 4. After an initial nonlinear region, due to the progressive reduction of the initial clearances between the sample and loading plate, the applied stress increases linearly with the displacement until a slight and gradual stiffness reduction, due to local out-of-plane instabilities of the laminate at the damaged area, may be observed before the final failure, especially for intermediate and high impact energies. A sequence of sudden load drops, which signal the propagation of localized fibre failures around the indentation area, is also visible immediately before the collapse in the response of specimens impacted at high energies. We also notice that while the force-displacement curves of unpinned and pinned laminates have comparable initial slopes when subjected to low-energy impacts,

unpinned samples exhibit larger reductions of initial stiffness for higher impact energies. This behaviour is a direct consequence of the growing difference in damage extent between unpinned and pinned laminates with increasing impact energy (see the graphs of fig. 3).

The CAI strength (defined as the maximum load measured during the test divided by the cross-sectional area of the specimen) of unpinned and z-pinned specimens of the two layups is reported as a function of impact energy in the graphs of fig. 5. We may see that the CAI strength values, independently of the layup and of the presence of Z pins, follow the same trend, with a first region in the low to intermediate energy range (i.e., for impact energies up to about 15 J) characterized by a decline with increasing impact energy, followed by a high energy region (impact energies larger than ~15 J) in which the strength tends to level off to a plateau value. We immediately notice that these two regions correspond to the two different damage scenarios previously described for the impacted samples. Therefore, the post impact compressive strength of the laminates appears strongly controlled by the key damage modes generated by the impact in dependence of the energy regime (i.e., respectively delaminations in the low to intermediate energy range and fibre fracture in association with major delaminations in the high energy range).

If we now compare the CAI strengths of control and z-pinned laminates across the whole range of applied impact energies, we notice that, irrespective of the layup, z-pinned laminates perform worse than analogous unpinned samples for impact energies less than about 5 J, but always better for intermediate and high impact energies. As an example, z-pinning increases the post-impact strength of both layups by about 20% for the high impact energy range corresponding to perforation damage.
The post-impact performances of z-pinned specimens also appear generally less sensitive to changes of impact energy than those of unpinned specimens, as shown by the smaller and more gradual decrease of their residual strength over the range of examined impact energies. For instance, the CAI strength of z-pinned $[0_2/90_2]_S$ samples reduces by about 40% when the impact energy is raised from 2 J to 30 J, as opposed to a drop of more than 55% for unpinned samples of the same layup. A similar trend may be observed in the CAI response of the $[0/\pm45/90]_S$ laminate.

A comparison of the impact damage areas and the CAI strength values reported in the graphs of fig. 3 and fig. 5 shows that the effect of z-pinning on the post-impact compression performance of the laminates cannot be simply explained by the reduction in the impact-induced delamination area. Different failure

mechanisms are therefore likely to play a role in the post-impact response of the laminates depending on the level of the applied impact energy.

To examine the progression of deformation and fracture events leading to the final collapse of unpinned and pinned laminates under compressive loadings, the front (impact) and rear faces of the samples were monitored during the CAI tests by digital cameras. Images of the surfaces extracted at relevant stages were subsequently examined to identify the occurring damage modes, with the aim of assessing the role of z-pins and evaluating the influence of pre-existing impact damage on the compressive response of the laminates.

Typical sequences of critical damage events are illustrated in figs 6-13 for CAI tests on unpinned and pinned $[0_2/90_2]_S$ samples.

Fig. 6 illustrates the progression of CAI damage observed on the rear face of an unpinned $[0_2/90_2]_S$ laminate impacted at 6 J, as representative of the compressive response of samples impacted in the intermediate energy regime. X-radiographs of the same specimen taken after impact and after the CAI test are shown in fig. 7. We may see in fig. 6 that the delaminated region of the 0° layers at the rear side of the sample start deflecting out-of-plane under compression, with the formation of an evident bulge that protrudes from the surface of the sample. The localized stiffness loss associated with this local buckling is expected to lead to a transfer of load from the central damaged area to the undamaged lateral regions of the laminate, with an increase in stress at the edge of the buckled delaminated area. The stress concentration occurring at the periphery of the buckled sublaminate triggers the initiation of fibre fracture on the 0° layers of the back side, with broken fibres quickly propagating by kinking and transverse shear failure to the specimen edges, finally leading to collapse of the laminate. The CAI response of unpinned laminates impacted with energies in the low to intermediate range is therefore governed by the size of the most critical delamination produced by the impact (i.e., that developing on the back 90°/0° interface), with larger delamination sizes corresponding to lower critical buckling loads and thus to worse CAI performances. It is worth noting that, contrary to what was reported in other studies [19, 22], no significant growth of the pre-existing impact-induced delaminations could be detected during the tests before the ultimate collapse. This finding is confirmed by the radiographs of fig. 7, which compare the damage induced by the impact (fig. 6a) with that generated by the CAI load (fig. 7b), where the new delaminations visible in the proximity of the post-CAI fibre failure path occur as a consequence of the failure of the 0° load bearing fibres.

The residual strength properties of unpinned $[0_2/90_2]_S$ laminates impacted at high energy levels, in contrast, appear to be greatly affected by the localized damage occurring at the indentation area, which consists of extensive fibre failures that initiate at the impact side and result in significant permanent indentations (figs. 8-9). The clusters of broken 0° fibres generated by the impact on the front face of the sample act as critical stress risers and further stress magnifications are due to the bending introduced by the residual dent and to the load transfer caused by buckling of the delaminated region. The damage evolution directly observed on the front side of a sample impacted at 24 J, illustrated in fig. 8, shows that the presence of pre-existing fibre fracture sites plays a primary role in the process leading to the collapse of the sample. As seen in fig. 8, the CAI failure is controlled by a fibre-dominated mechanism, where compressive fibre fracture initiates at or near the tips of pre-existing 0° fibre cracks and propagates along a path that grows transversally up to the lateral edges of the specimen. It is worth remarking that, again, the initial impact delaminations do not significantly propagate across the laminate width before the final collapse, as visible in the X-radiographs of damage of fig. 9.

The development of damage events observed under compressive load on the surfaces of z-pinned $[0_2/90_2]_S$ samples is shown in figs. 10-13. The figures illustrate the CAI responses of z-pinned samples impacted at the same energy levels previously examined for the unpinned samples, respectively representative of intermediate (6 J) and high (24 J) impact energies.

Fig. 10 shows that, unlike unpinned $[0_2/90_2]_S$ laminates, no evident out-of-plane deflections may be seen, even at the maximum load attained during the test, on the rear surface of the z-pinned sample impacted at an intermediate energy level (6 J). This is a direct consequence of the beneficial effect of z-pins, which not only reduce the size of the impact-induced delamination area, but also provide bridging tractions across the delaminated interfaces during CAI loading, therefore tying the sublaminates of the damaged region together and inhibiting or delaying the out-of-plane instability of the delaminated regions. The load redistribution effect associated with localized buckling is then prevented or greatly mitigated compared to that of unpinned laminates, which translates into an increase in the CAI strength of the laminate after z-pinning. A significant role in the mechanisms controlling the CAI performance of the z-pinned laminate is however played by the presence of the typical microstructural defects generated by the insertion of z-pins [1, 13], such as broken fibres, fibre waviness and resin-rich regions, which promote fibre fracture and reduce the compressive strength of the original laminate. It is actually seen in fig. 10 that the failure of the

laminate is initiated at a pin location by the formation of a cluster of broken fibres, which subsequently grow in an unstable way across the sample width following paths that join adjacent z-pin sites (fig. 11). The damage mechanisms governing the CAI performance of z-pinned $[0_2/90_2]_S$ laminates impacted at high energies (figs 12-13) are similar to those observed in unpinned laminates. As in analogous unpinned samples, the damage induced by impact is characterized by significant fibre fracture at the impact region and by a deep residual indentation as seen in fig. 12. The compressive fibre failure that leads to the final collapse under CAI loading appears to be triggered by the stress concentrations at the tip of pre-existing clusters of impact-induced broken fibres. In comparison to unpinned samples, however, the smaller impact-induced delamination areas (fig. 13) and the bridging forces provided by z-pins across sublaminates are expected to result in a more gradual load redistribution between the damaged and the undamaged region, which translates to improved CAI strength properties.

The damage features and failure processes observed during CAI tests in the quasi-isotropic $[0/\pm45/90]_S$ laminates are basically the same as those just illustrated for the cross-ply $[0_2/90_2]_S$ samples. As an example, Figs. 14-17 show the impact and CAI damage scenarios and the key damage events observed during CAI tests on unpinned (figs. 14, 15) and pinned (figs. 16, 17) $[0/\pm45/90]_S$ samples previously impacted at 8 J. We may again notice that while the CAI strength of the unpinned laminate is controlled by the buckling of the delaminated plies at the rear side of the sample (fig. 14), the failure process of the pinned laminate is initiated on the front side by the onset of 0° fibre failure at z-pin sites (fig. 16). Moreover, as already observed in cross-ply laminates, the delaminations induced by impact do not significantly grow under compressive loads, neither in unpinned (fig. 15) nor in z-pinned (fig. 17) laminates.

The general features and descriptions provided for the post-impact behaviour of the $[0_2/90_2]_S$ samples remain therefore essentially valid for the quasi-isotropic $[0/\pm45/90]_S$ layup.

The information acquired through visual inspection and X-radiography helps clarify the mechanisms by which the post-impact performance of the laminates is affected by z-pinning. The sequence of events identified during the analyses also allows to explain the characteristic trends seen in the plots of fig. 5, which show that the effect of z-pinning on the CAI strength is detrimental in the low energy regime and beneficial in the intermediate to high energy regime.

The experimental observations show that the amount of damage induced by low-energy impacts (energy less than about 5 J) is so small that it cannot significantly affect the CAI response of unpinned laminates.

In the presence of this damage scenario, z-pinning is not capable of providing any improvement, since the bridging mechanism of z-pins cannot be efficiently activated by short delamination cracks. Therefore, the CAI failure of z-pinned laminates in the low energy range is governed mainly by the localised manufacturing damage arising from the pinning process, which induces stress concentrations that reduce the compressive strength of the load bearing 0° layers.

In contrast, impacts with intermediate energies (i.e., approximately between 5 and 15 J) generate delaminated areas at individual interfaces that are large enough to allow the formation of a large-scale z-pin bridging zone, which leads to smaller impact-induced delaminations and increased post-impact flexural stiffnesses of the damaged region in comparison to unpinned laminates. Therefore, while the CAI collapse of unpinned laminates is governed by buckling of the delaminated regions, in z-pinned laminates the local buckling is delayed, or even inhibited, and a key role in the CAI failure process is again played by the stress concentrations associated to the microstructural defects around z-pin sites. The prevention of local out-of-plane instabilities, with the ensuing change in the failure-triggering mechanism, is thus the primary factor for the significant improvement in CAI strength of z-pinned laminates over base laminates.

When the impact energy exceeds the threshold for perforation (i.e., for impact energies larger than about 15 J), the damage induced by impact in both pinned and unpinned laminates is characterized, in addition to extensive delaminations, by major fibre fracture localized at the indentation area. The stress concentrations produced by the impact-induced fibre failures play the principal role in controlling the residual strength of the laminates. This localised effect explains why the CAI strengths of both unpinned and pinned laminates are practically independent of the extent of the delaminated area in the perforation damage range. The better CAI performance of z-pinned laminates in comparison with unpinned laminates can be again accounted for by the higher residual stiffness of the delaminated region, which results in a reduced transfer of load from the damaged central region to the undamaged lateral ligaments and thus in a smaller stress amplification in the 0° load carrying layers at the edge of the indentation area.

## 4. Conclusions

The effect of z-pinning on the CAI performance of thin $[0_2/90_2]_S$ and $[0/\pm 45/90]_S$ carbon-epoxy laminates was investigated in this study over the full range of impact damage severities that may be induced by low-velocity impacts. The development of the critical damage mechanisms leading to CAI failure was

examined by visual observations and by X-radiography to characterize the role of z-pins and their interaction with impact damage in the CAI response of the laminates.

The following main conclusions may be drawn from the study:

- Two main scenarios of impact-induced damage may be recognized in the laminates depending on the level of impact energy. Damage generated by impacts with low to intermediate energy (impact energy less than approximately 15 J) mainly consists of delaminations and matrix damage, while higher energy impacts cause perforation damage, where extensive fibre failures develop at the indentation area in addition to widespread delaminations. z-pins reduce the size of delaminations only for impacts with energy high enough to induce delamination cracks sufficiently long to allow the formation of a large-scale z-pin bridging zone.

- The CAI strength of all samples, irrespective of the layup and of the presence of z-pins, decreases with increasing impact energy after impacts in the low to intermediate energy range (2-15 J), which are associated with the damage scenario consisting of delaminations and matrix cracks. The CAI strength of the samples levels off to a plateau value for higher impact energies, which correspond to perforation damage conditions, characterized by major fibre fracture localized at the indentation area.

- In both cross-ply and quasi-isotropic laminates, the CAI strength is degraded by z-pins for low impact energies (less than about 5 J), but improved for intermediate to high impact energies (above~5 J). Increases in CAI strength of about 20% are for example observed in the plateau region corresponding to perforation damage.

- The role of z-pins on the CAI response of the laminates is influenced by the different deformation and damage mechanisms that occur during compressive loading, which, in turn, are strongly dependent on the nature and extent of the damage induced by impact. As a result, z-pins may have an adverse or beneficial effect depending on the energy of the impact imparted to the laminate .

Low-energy impacts (below 5 J) induce very small damage amounts, which cannot significantly affect the CAI strength of unpinned laminates; within this energy range, z-pins are detrimental to the CAI properties, since, while their potential traction forces cannot be effectively exploited, the manufacturing defects around z-pin sites promote the early initiation of the CAI failure process.

Impacts in the intermediate energy regime (in the range of 5-15 J) lead to delamination sizes large enough to activate the bridging mechanism of z-pins, with a substantial reduction of delaminated areas in

pinned laminates. As a consequence, while the buckling of delaminated plies controls the CAI performance of unpinned laminates, local out-of-plane instabilities are effectively restrained in z-pinned laminates, thus resulting in a clear improvement of CAI strength over base laminates.

The CAI failure process of both unpinned and pinned samples impacted in the high-energy perforation regime (above ~15 J) is dominated by the local stress concentration associated with the extensive fibre failure at the indentation area, which accounts for the limited dependence of CAI strength on impact energy in this energy range. The superior CAI properties of z-pinned laminates can be attributed to the higher stiffness of the damaged region, which contributes to a more uniform stress distribution on the load bearing 0° layers across the undamaged ligaments.

Further work is required to examine several aspects not considered in the study, such as the effect of laminate thickness or the influence of pin size, shape and density on the specific failure mechanisms that lead to final CAI collapse for the different impact damage severities.

**Author contributions**
The authors have contributed equally to the manuscript

## References


**1** Tong L, Mouritz AP, Bannister MK. 3D fibre reinforced polymer composites. Oxford: Elsevier; 2002

**2** Sridharan S. (Ed.). Delamination behaviour of composites. Cambridge: Woodhead Publishing Limited, 2008.

**3** Dell'Anno G, Cartié DD, Partridge IK, Rezai A. Exploring mechanical property balance in tufted carbon fabric/epoxy composites. Compos A Appl Sci Manuf 2007;38(11):2366–73.

**4** Francesconi L, Aymerich F. Numerical simulation of the effect of stitching on the delamination resistance of laminated composites subjected to low-velocity impact. Compos Struct 2017;159:110–20

**5** Yu J, Zhou C, Li S. Experimental and numerical research on the mode I delamination of looped fabric reinforced laminate. Comp B 2020; 182: 107566.

**6** Partridge IK, Cartié DDR, Bonnington T. Manufacture and performance of z-pinned composites. In: Advani S, Shonaike G, editors. Advanced polymeric materials: structure-property relationships. Boca Raton: CRC Press; 2003.

**7** Knopp A, Scharr G. Effect of z-pin surface treatment on delamination and debonding properties of z-pinned composite laminates. J Mat Sci 2014; 49: 1674–83.

**8** Pingkarawat K, Mouritz AP. Improving the mode I delamination fatigue resistance of composites using z-pins. Comp Sci Tech 2014; 92:70–6.

**9** Pegorin F, Pingkarawat K, Mouritz AP. Mixed-mode I/II delamination fatigue strengthening of polymer composites using z-pins. Comp B 2017; 123: 219–26.

**10** Pegorin F, Pingkarawat K, Daynes S, Mouritz AP. Influence of z-pin length on the delamination fracture toughness and fatigue resistance of pinned composites; Comp B 2015; 78: 298-307.

**11** Partridge IK, Cartie DDR. Delamination resistant laminates by Z-Fiber pinning: Part I manufacture and fracture performance. Compos A Appl Sci Manuf 2005; 36: 55–64.

**12** Mouritz AP, Cox BN. A mechanistic interpretation of the comparative in-plane mechanical properties of 3D woven, stitched and pinned composites. Compos A Appl Sci Manuf 2010; 41(6):7 09–28.

**13** Mouritz AP. Review of z-pinned laminates and sandwich composites. Compos A Appl Sci Manuf 2020; 139: 106128.

**14** Cartie DDR, Troulis M, Partridge IK. Delamination of z-pinned carbon fibre reinforced laminates. Comp Sci Tech 2006; 66: 855–61

**15** Chang P, Mouritz AP, Cox BN. Properties and failure mechanisms of pinned composite lap joints in monotonic and cyclic tension. Compos A Appl Sci Manuf 2006;66:2163–76.

**16** Li M, Chen P, Kong B, Peng T, Yao Z, Qiu X. Influences of thickness ratios of flange and skin of composite T-joints on the reinforcement effect of z-pin. Comp B 2016; 97: 216e225.

**17** Koh TM, Isa MD, Feih S, Mouritz AP. 2013. Experimental assessment of the damage tolerance of z-pinned T-stiffened composite panels. Comp B 2013; 44(1): 620-627.

**18** Rezai A, Cartie´ D, Partridge I, Irving P, Ashton T, Negre P, Langer J. Interlaminar damage resistance of Z-Fiber reinforced structural CFRP. In: Proceedings ICCM 13, 13th International Conference on Composite Materials, June 2001, Beijing (China).

**19** Zhang X, Hounslow L, Grassi M. Improvement of low-velocity impact and compression-after-impact performance by z-fibre pinning. Compos Sci Technol 2006; 66: 2785–94.

**20** Isa MD, Feih S, Mouritz AP. Compression fatigue properties of z-pinned quasi-isotropic carbon/epoxy laminate with barely visible impact damage. Compos Struct 2011; 93: 2269-2276.

**21** Mouritz AP. Delamination properties of z-pinned composites in hot–wet environment. Compos A Appl Sci Manuf 2013; 52:1 34–42.

**22** Knaupp M, Baudach F, Franck J, Scharr G. Impact and post-impact properties of CFRP laminates reinforced with rectangular z-pins. Compos Sci Technol 2013; 87: 218–23.

**23** Francesconi L, Aymerich F. Effect of z-pinning on the impact resistance of composite laminates with different layups. Compos A Appl Sci Manuf 2018; 114: 136-148.

**24** Wisnom MR. The role of delamination in failure of fibre-reinforced composites. Philos Trans R Soc A Math Phys Eng Sci 2012; 370(1965): 1850–70.

**25** Childress JJ, Freitas GA. Z-direction pinning of composite laminates for increased survivability. AIAA 1992-1099. Proceedings of the 1992 Aerospace Design Conference, February 1992, Irvine, CA (USA).

**26** Ranatunga V, Crampton SM, Clay SB. Assessment of damage tolerance and static residual strength of Z-pin reinforced composites. Proceedings of AIAA Scitech 2019 Forum.

**27** Isa MD. Experimental assessment of the damage tolerance of z-pinned aerospace composites, PhD thesis, RMIT University, Melbourne, 2013.

**28** Pegorin F. An Experimental Investigation of Multi-Functional Z-Pinned Carbon-Epoxy Composites, PhD Thesis, RMIT University, Melbourne, 2016.

**29** Knopp A, Funck E, Holtz A, Scharr G. Delamination and compression-after-impact properties of z-pinned composite laminates reinforced with circumferentially notched z-pins. Compos Struct 2022; 285: 115188.

**30** ASTM D7137/D7137M-12. Compressive residual strength properties of damaged polymer matrix composite plates, ASTM International, West Conshohocken, PA, doi: 10.1520/D7137_D7137M-12.

**31** Nettles AT. The effects of embedded internal delaminations on composite laminate compression strength; an experimental review. NASA TM-10B440, 1994.

**32** Remacha M, Sánchez-Sáez S, López-Romano B, Barbero E. A new device for determining the compression after impact strength in thin laminates. Compos Struct 2015; 127: 99–107.

**33** Yasaee M, Mohamed, G.; Pellegrino A, Petrinic N, Hallett SR. Strain rate dependence of mode II delamination resistance in through thickness reinforced laminated composites. Int. J. Impact Eng. 2017: 1-11.

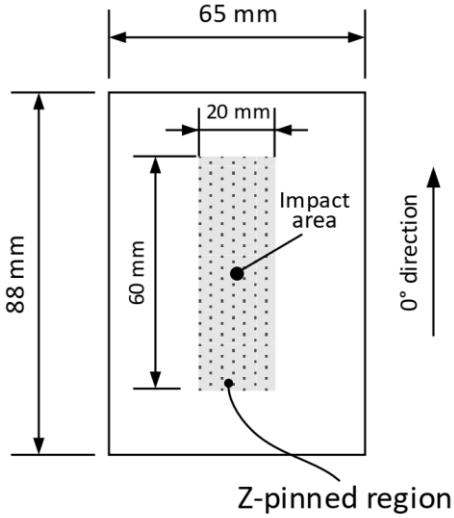


Fig. 1: Size and z-pinned region of samples.

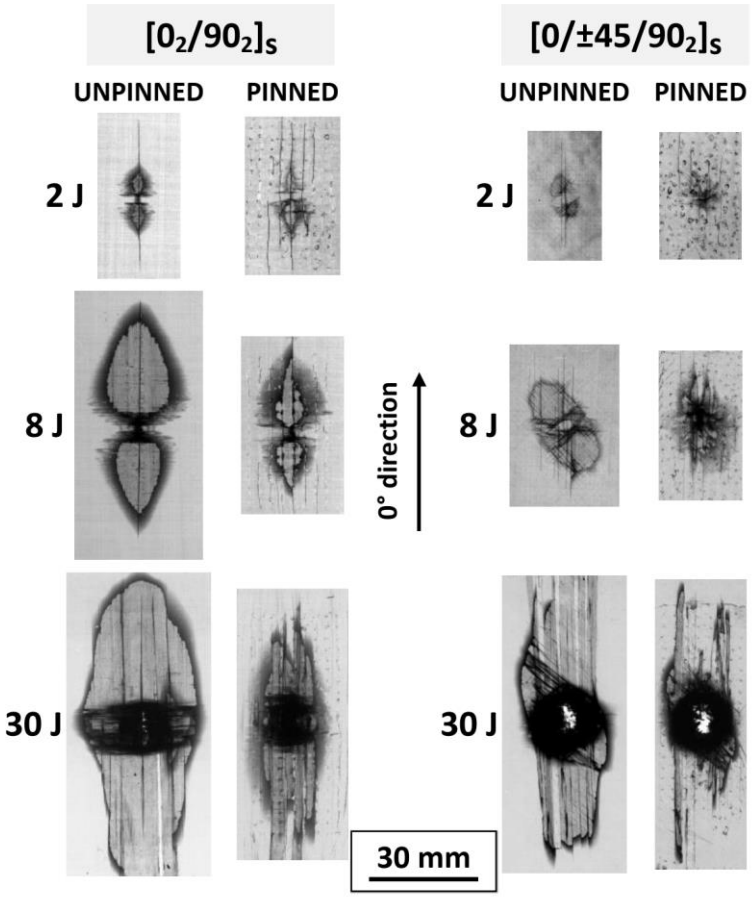


Fig. 2: X-radiographs of impact damage in unpinned and pinned $[0_2/90_2]_S$ and $[0/\pm45/90]_S$ samples impacted at 2 J, 8 J and 30 J.

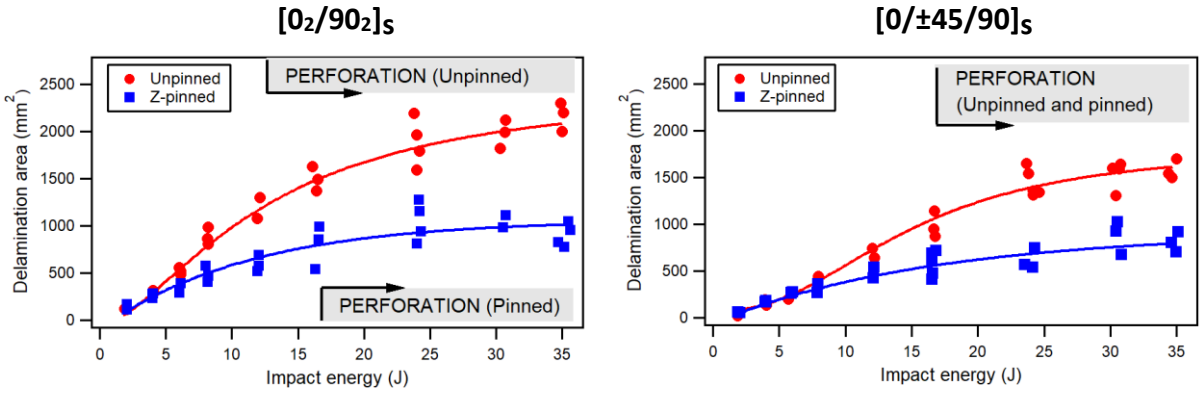


Fig. 3: Projected delamination areas induced by impact vs impact energy in unpinned and pinned $[0_2/90_2]_S$ (left) and $[0/\pm45/90]_S$ (right) samples.

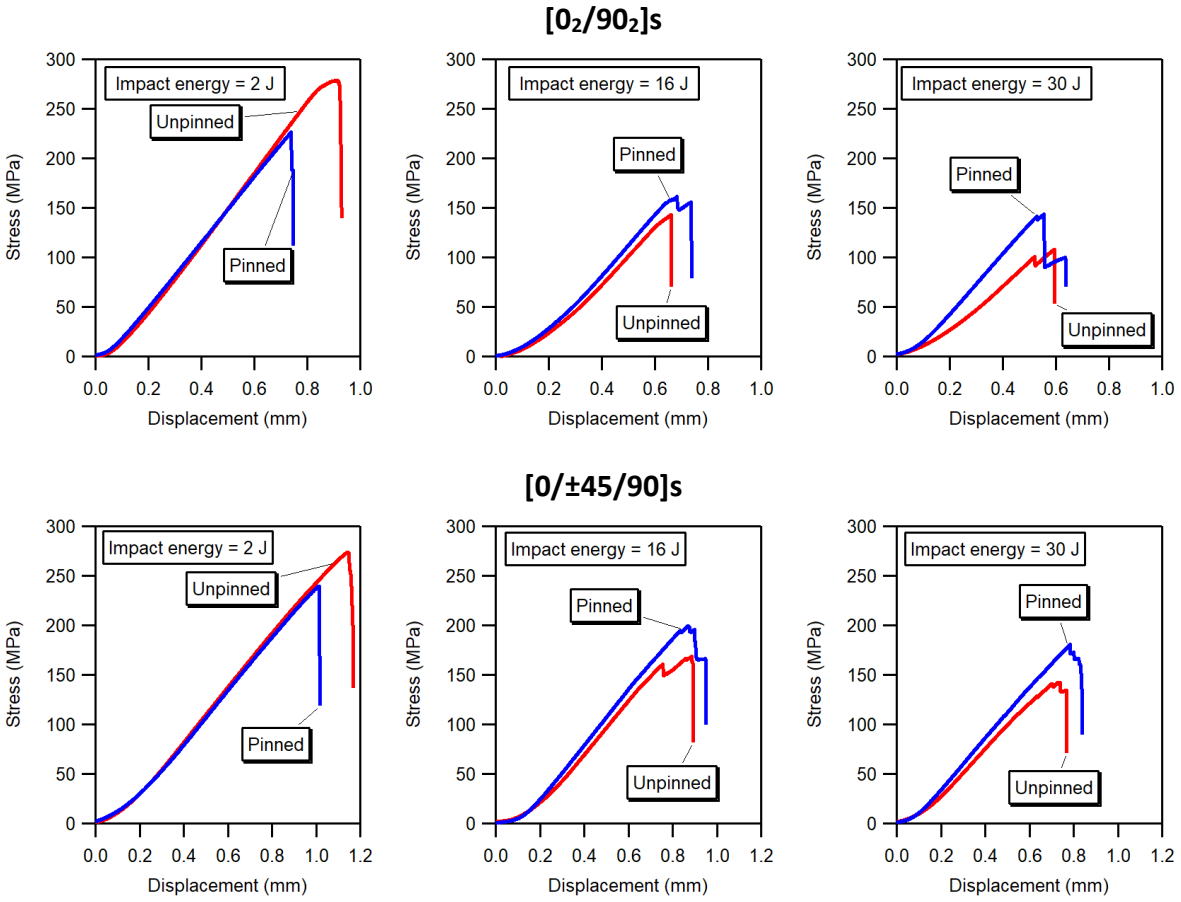


Fig. 4: Typical stress vs displacement curves recorded during CAI tests on unpinned and pinned $[0_2/90_2]_S$ (top) and $[0/\pm45/90]_S$ (bottom) samples.

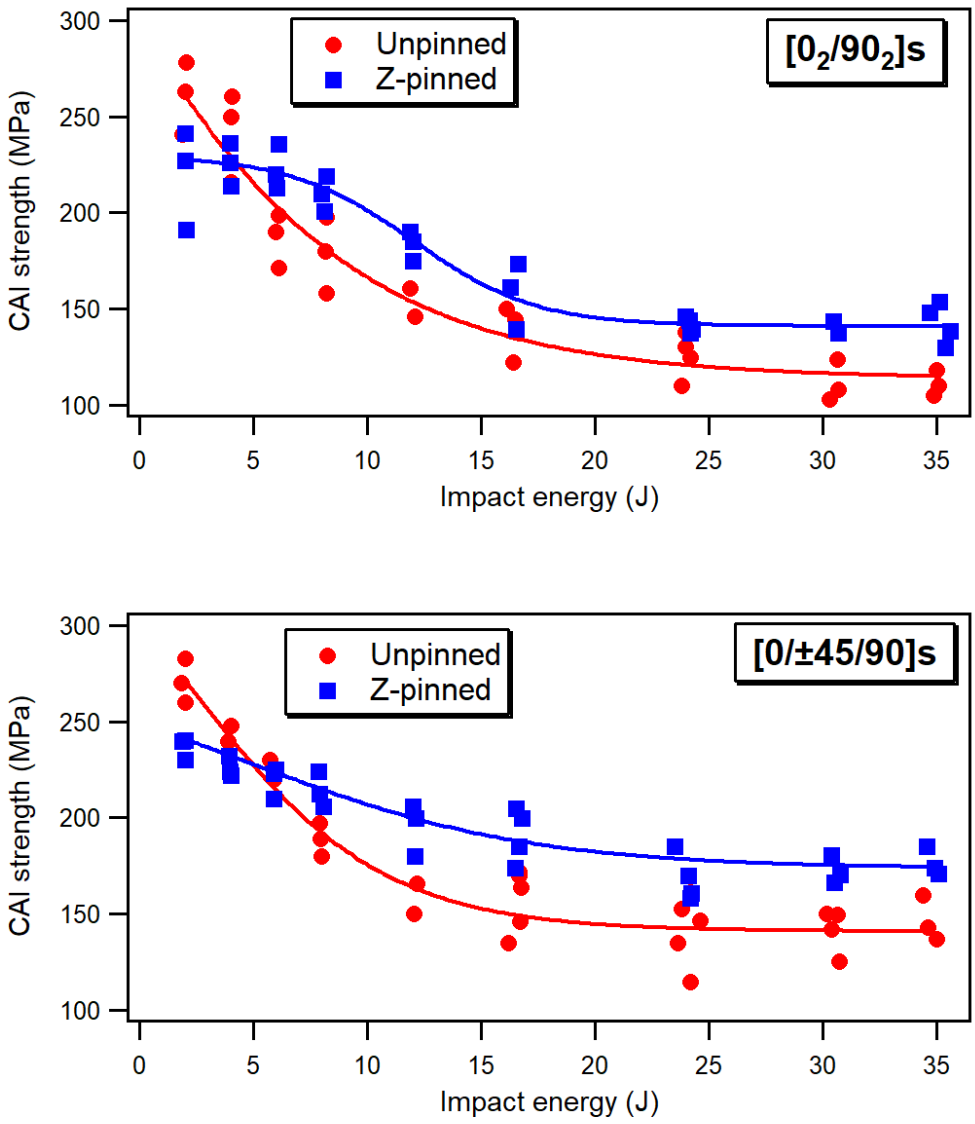


Fig. 5: CAI strength vs impact energy for $[0_2/90_2]_S$ (top), and $[0/\pm45/90]_S$ (bottom) samples.

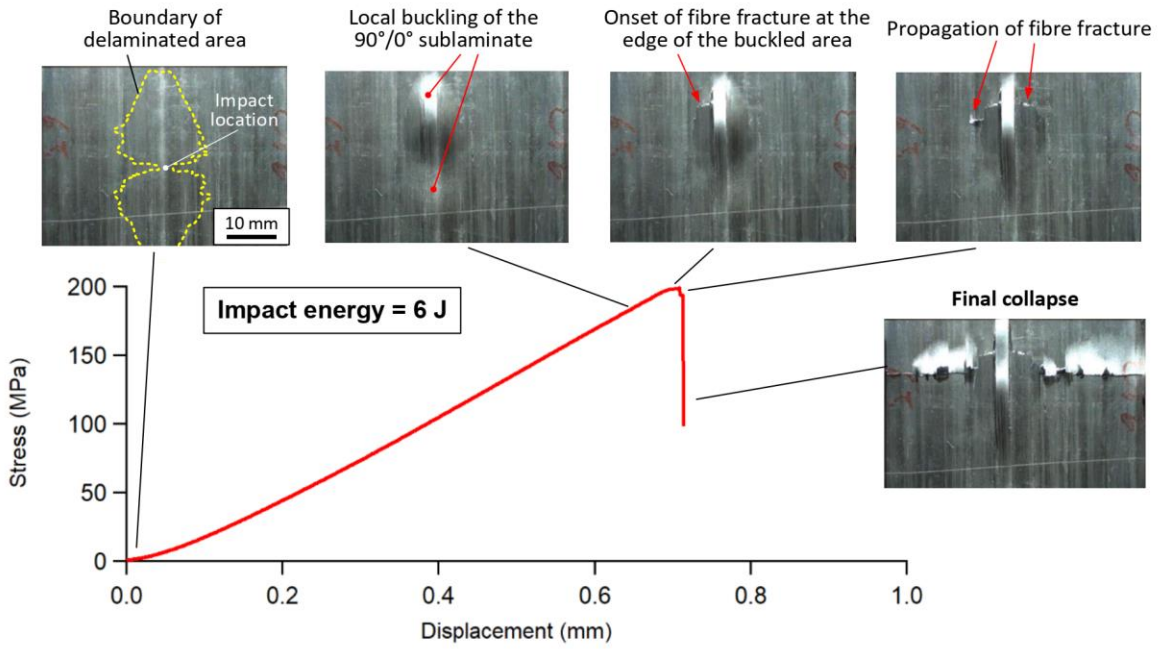


Fig. 6: Sequence of damage events observed during CAI loading on the rear face of an unpinned $[0_2/90_2]_S$ sample impacted at 6 J.

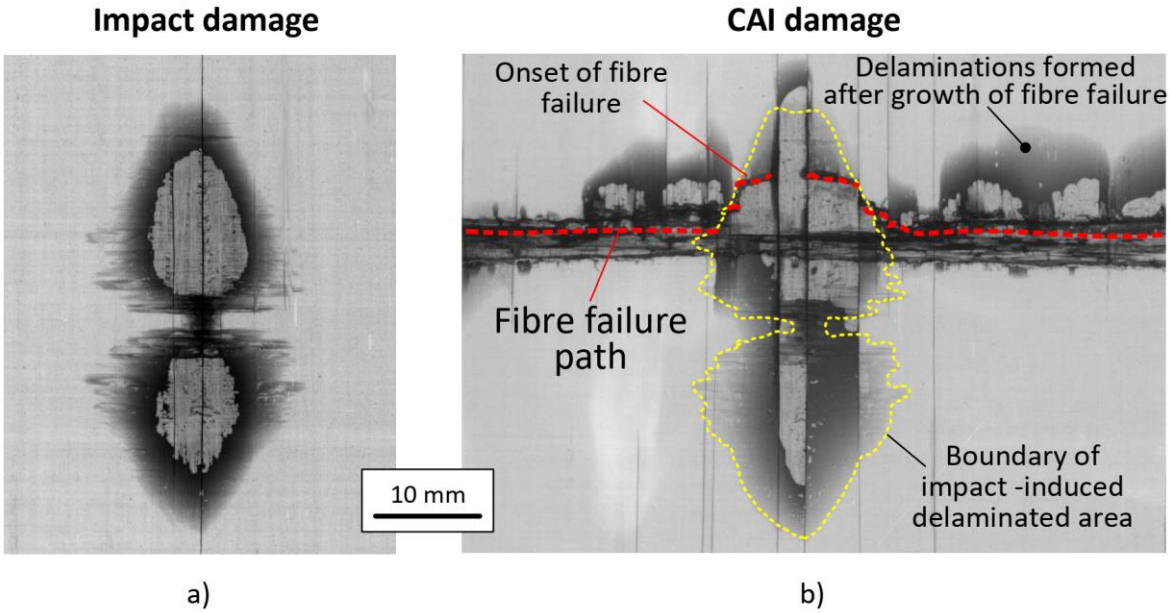


Fig. 7: X-radiographs of damage occurring after impact (a) and after CAI loading (b) in the unpinned $[0_2/90_2]_S$ sample shown in fig. 5 (impact energy = 6 J).

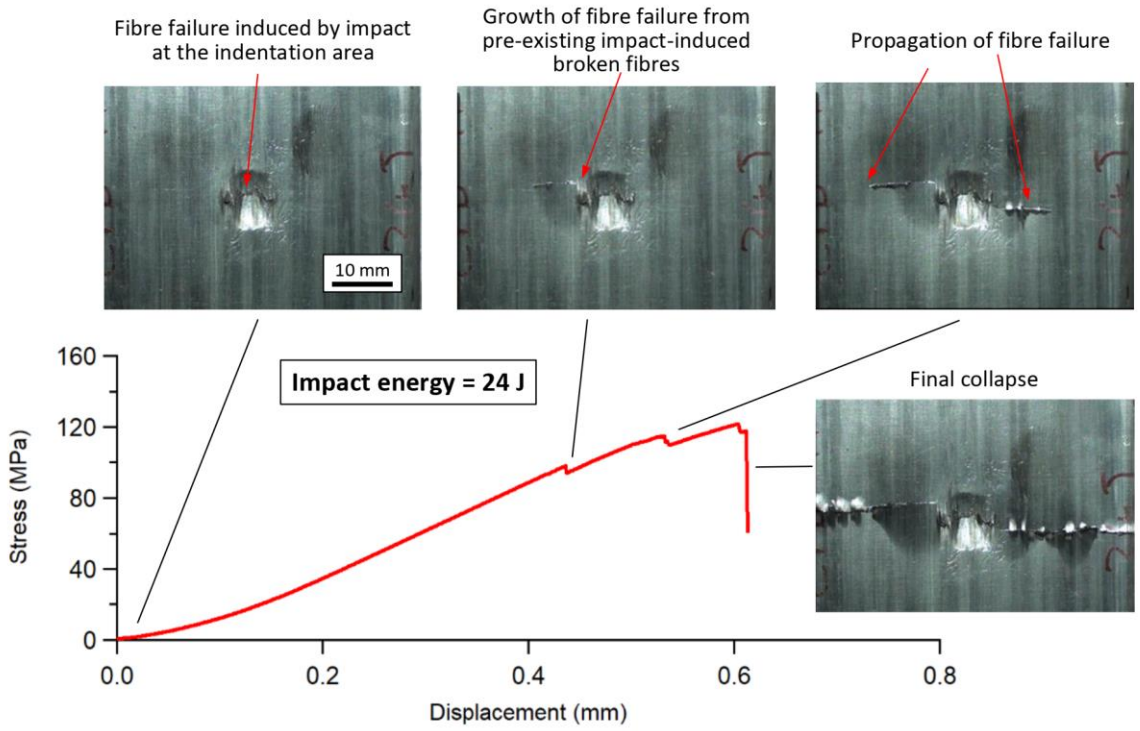


Fig. 8: Sequence of damage events observed during CAI loading on the front face of an unpinned $[0_2/90_2]_S$ sample impacted at 24 J.

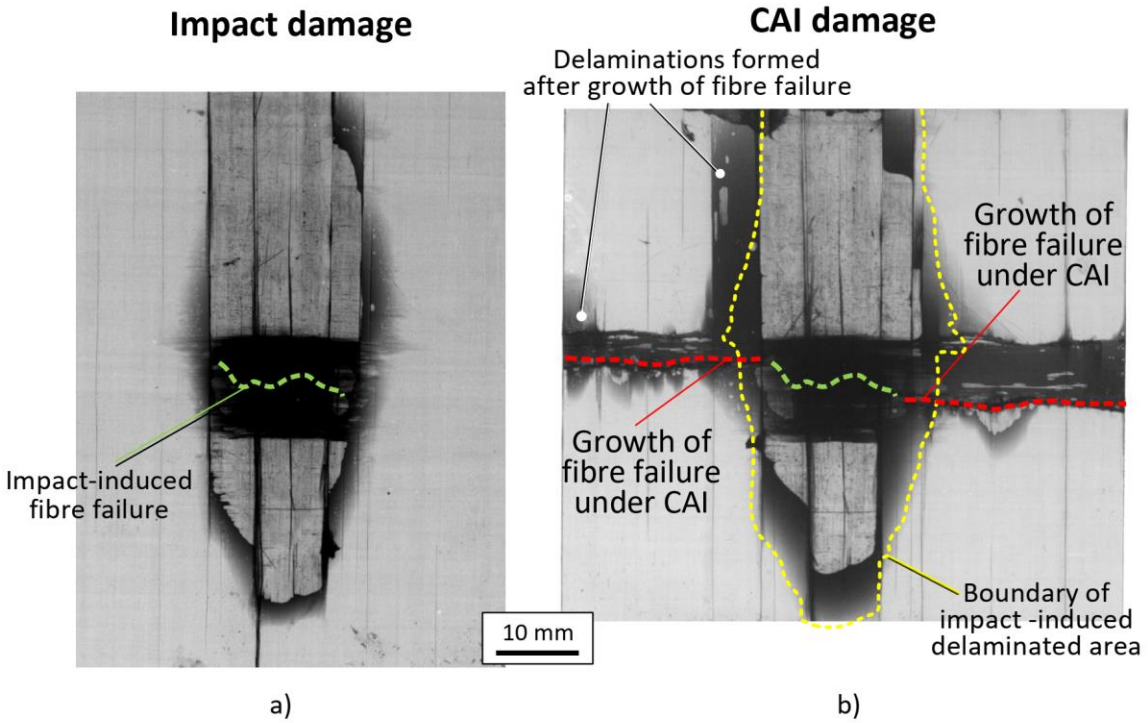


Fig. 9: X-radiographs of damage occurring after impact (a) and after CAI loading (b) in the unpinned $[0_2/90_2]$s sample shown in fig. 7 (impact energy = 24 J).

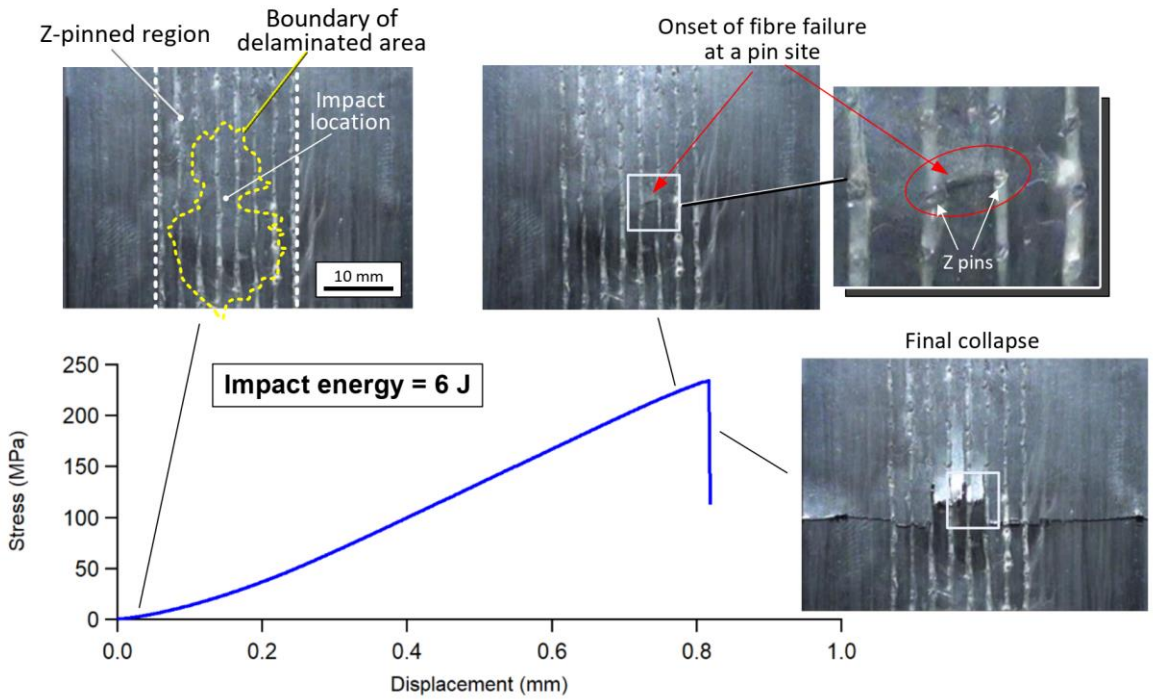


Fig. 10: Sequence of damage events observed during CAI loading on the rear face of a z-pinned $[0_2/90_2]$s sample impacted at 6 J.

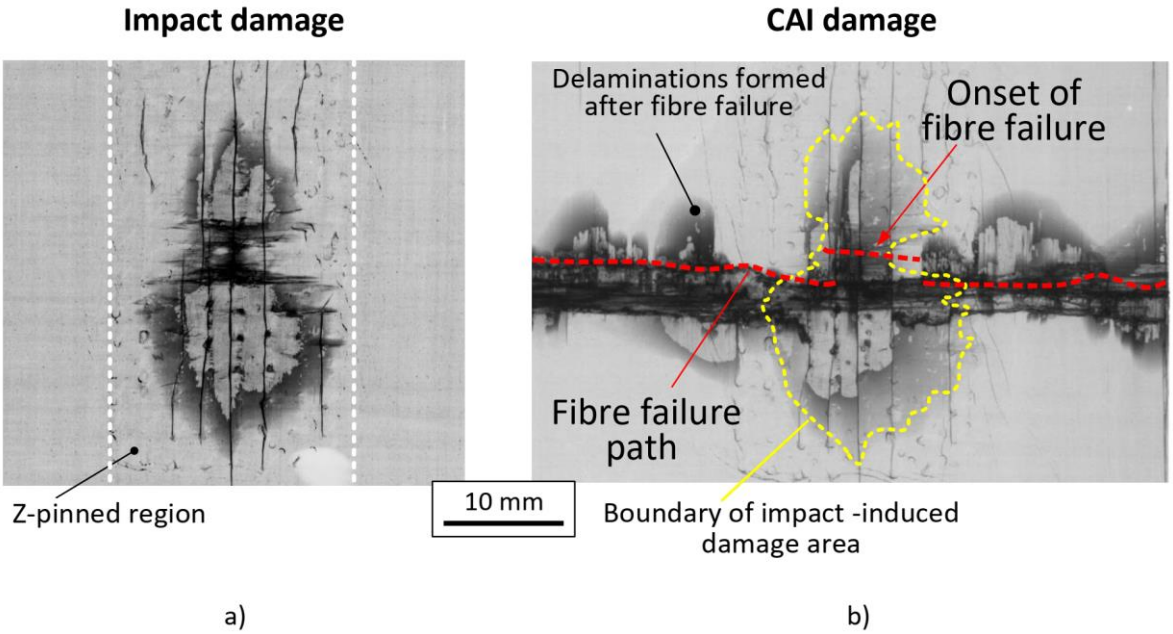


Fig. 11: X-radiographs of damage occurring after impact (a) and after CAI loading (b) in the z-pinned $[0_2/90_2]$s sample shown in fig. 9 (impact energy = 6 J).

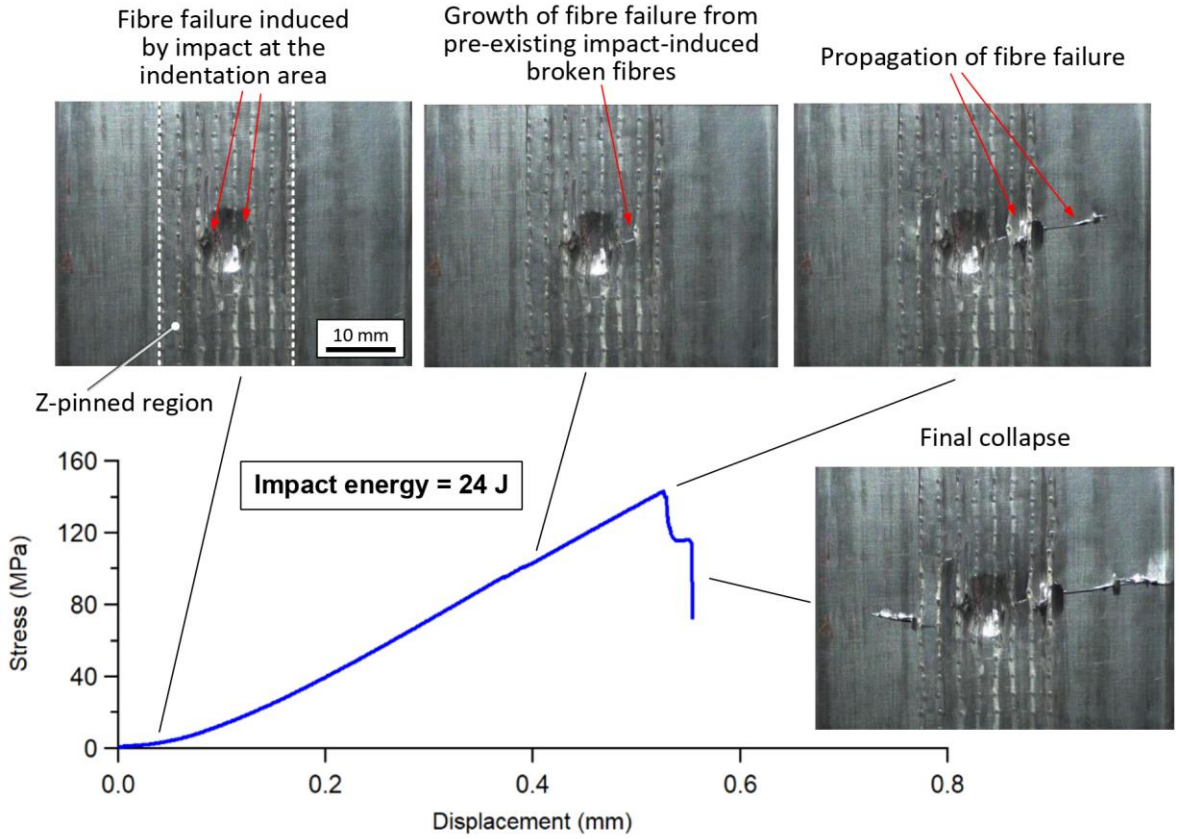


Fig. 12: Sequence of damage events observed during CAI loading on the front face of a z-pinned $[0_2/90_2]$s sample impacted at 24 J.

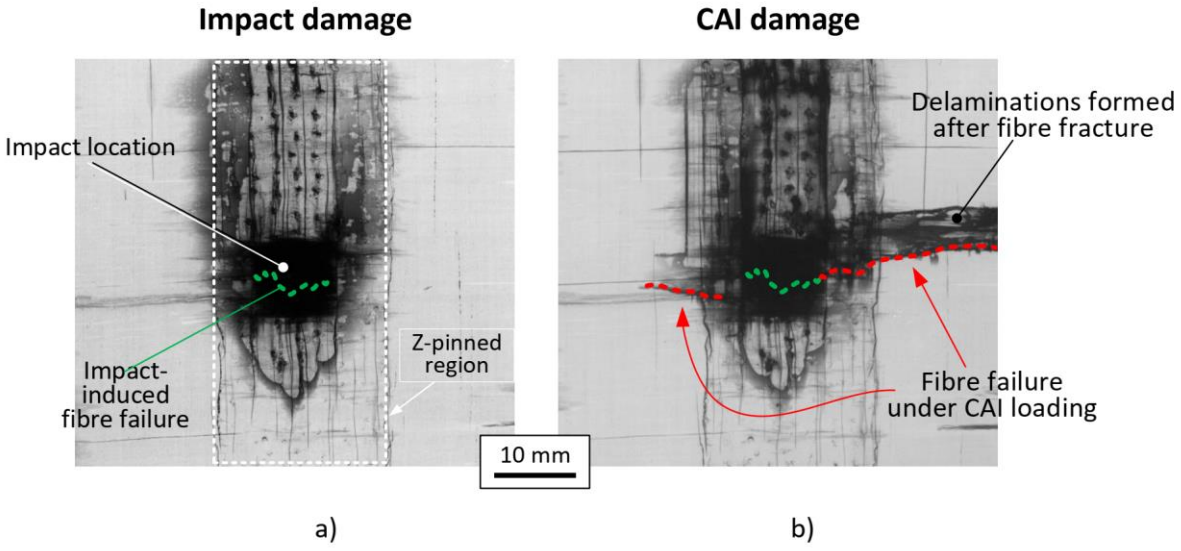


Fig. 13: X-radiographs of damage occurring after impact (a) and after CAI loading (b) in the z-pinned $[0_2/90_2]$s sample shown in fig. 11 (impact energy = 24 J).

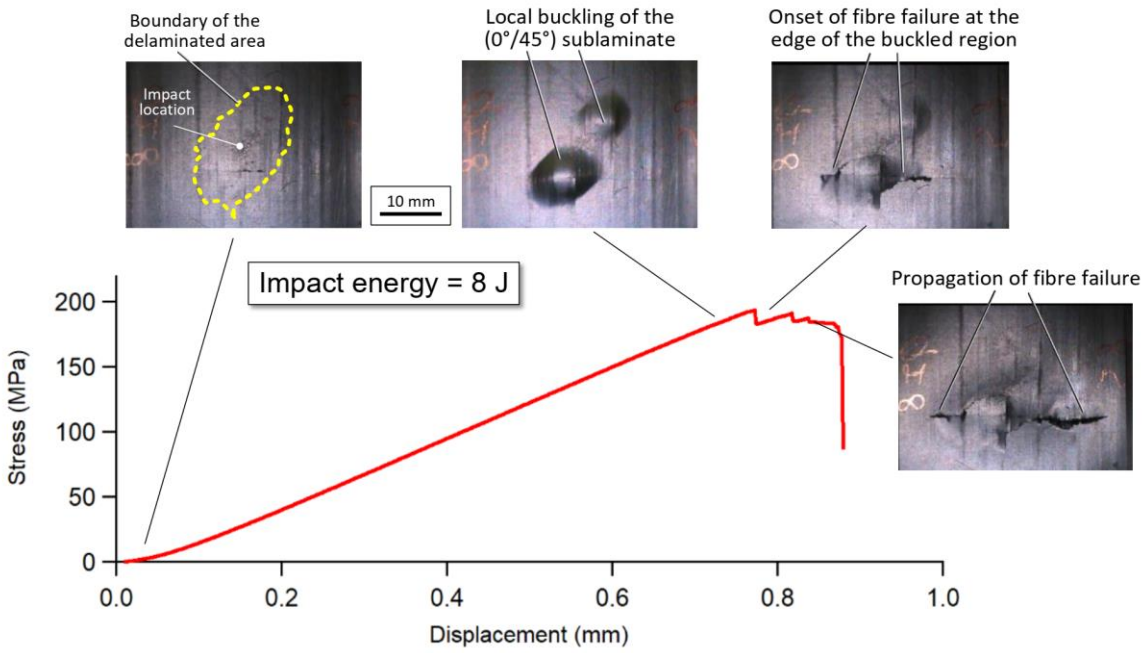


Fig. 14: Sequence of damage events observed during CAI loading on the rear face of an unpinned [0/±45/90]s sample impacted at 8 J.

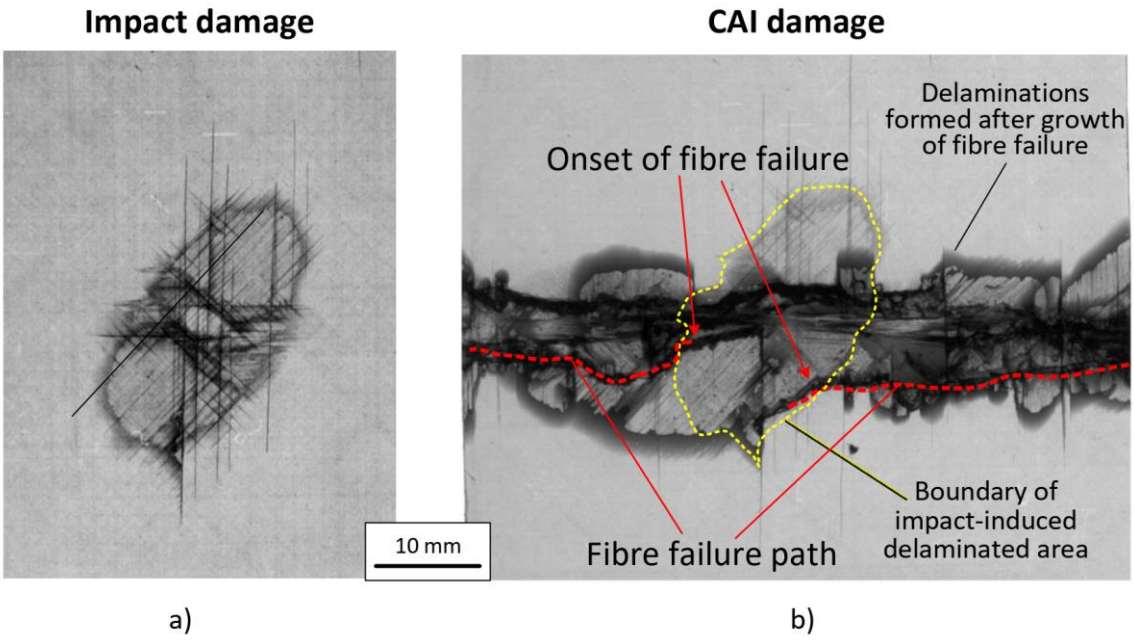


Fig. 15: X-radiographs of damage occurring after impact (a) and after CAI loading (b) in the unpinned [0/±45/90]s sample shown in fig. 13 (impact energy = 8 J).

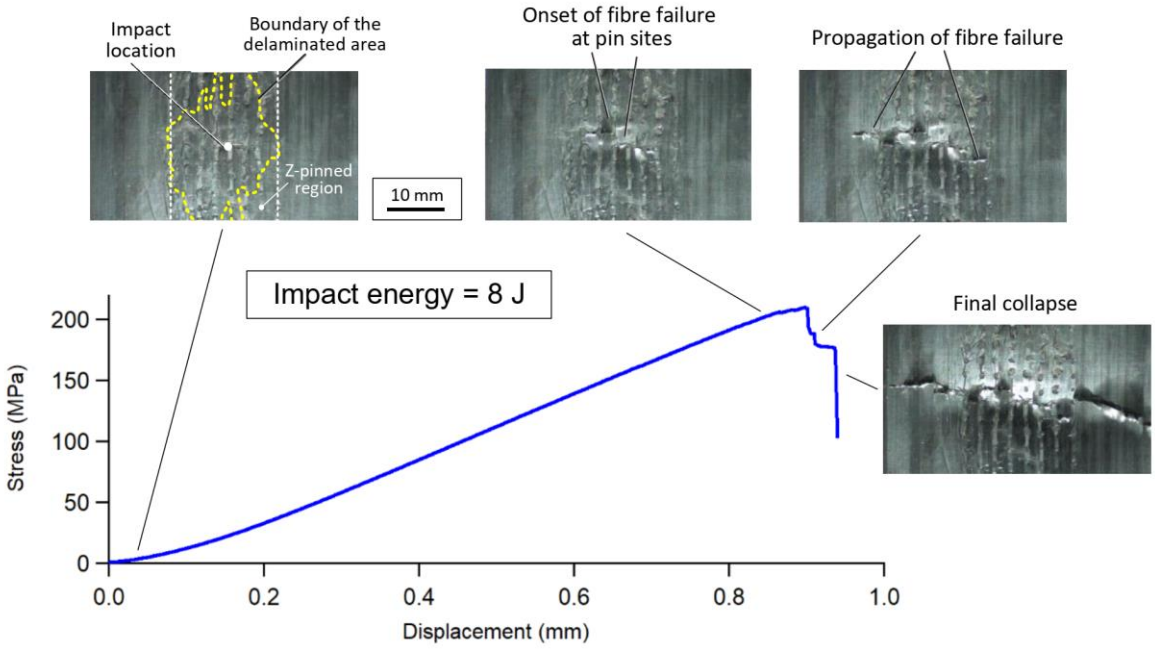


Fig. 16: Sequence of damage events observed during CAI loading on the front face of a z-pinned [0/±45/90]s sample impacted at 8 J.

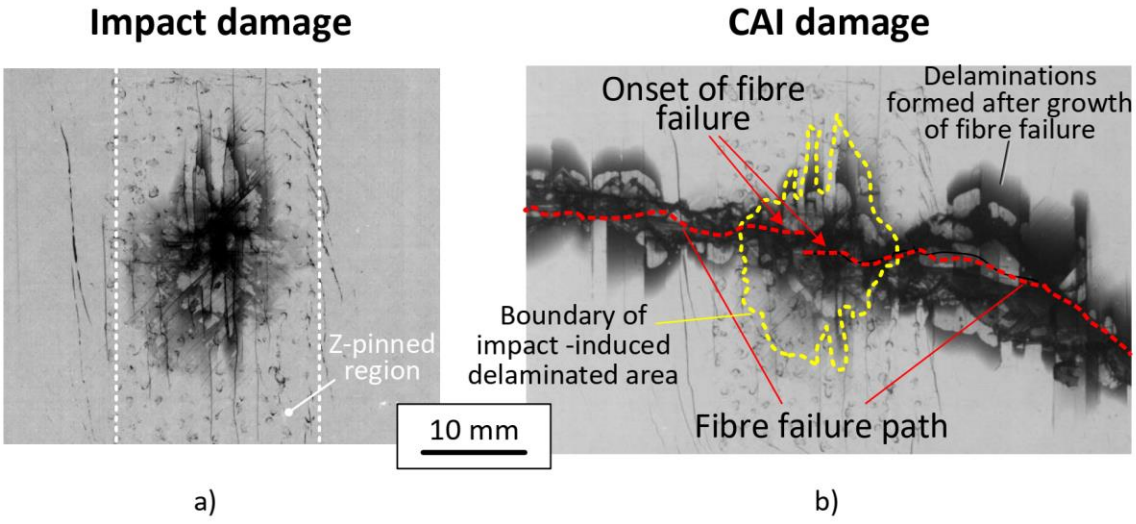


Fig. 17: X-radiographs of damage occurring after impact (a) and after CAI loading (b) in the z-pinned [0/±45/90]s sample shown in fig. 15 (impact energy = 8 J).

Table 1: Summary of tested samples

| | | | $[0_2/90_2]_S$ laminates | | $[0/\pm45/90]_S$ laminates | |
|---|---|---|---|---|---|---|
| Impact energy (J) | Drop height (m) | Impact velocity (m/s) | Number of unpinned samples | Number of z-pinned samples | Number of unpinned samples | Number of z-pinned samples |
| 2 | 0.089 | 1.33 | 3 | 3 | 3 | 3 |
| 4 | 0.179 | 1.87 | 3 | 3 | 3 | 2 |
| 6 | 0.269 | 2.29 | 3 | 3 | 2 | 3 |
| 8 | 0.358 | 2.65 | 3 | 3 | 3 | 3 |
| 12 | 0.537 | 3.24 | 2 | 3 | 2 | 3 |
| 16.5 | 0.738 | 3.80 | 3 | 3 | 4 | 4 |
| 24 | 1.074 | 4.59 | 4 | 4 | 5 | 4 |
| 30 | 1.343 | 5.13 | 3 | 2 | 4 | 3 |
| 35 | 1.567 | 5.54 | 3 | 4 | 3 | 3 |

Note: Impact energy, drop height and impact velocity columns report nominal values; slight differences may occur between the nominal values and the actual values measured on the single tests.